Discover Forests

RESEARCH

Open Access

Evaluating Sentinel-2 vegetation indices for aboveground biomass estimation and forest management in the fragmented Atlantic Rainforest

Felipe Góes de Moraes[1], Deicy Carolina Lozano-Sivisaca[1], José Raimundo de Souza Passos[2], Rafael Barroca Silva[1,3], Ludmila Ribeiro Roder[3], Antonio Ganga[3], Gian Franco Capra[3*] and Iraê Amaral Guerrini[1]

*Correspondence:
Gian Franco Capra
gfcapra@uniss.it
[1]Department of Forest, Soil and Environmental Sciences, College of Agricultural Sciences, São Paulo State University - UNESP, Botucatu, SP 18610-034, Brazil
[2]Biodiversity and Bioestatistic Department, Bioscience Institute (IBB), São Paulo State University (UNESP), Botucatu, São Paulo, Brazil
[3]Department of Architecture, Design, and Urban Planning, University of Sassari, Viale Piandanna 4, 07100 Sassari, Italy

Abstract
Accurate estimation of aboveground biomass (AGB) in tropical forests is essential for carbon accounting and effective forest conservation, particularly in the biodiverse and threatened Atlantic Rainforest. Satellite-derived vegetation indices (VIs) offer potential for large-scale assessment of forest biomass and condition. We evaluated the utility of four Sentinel-2-derived vegetation indices (normalized difference vegetation index (NDVI), enhanced vegetation index (EVI), ratio vegetation index (RVI), and optimized soil-adjusted vegetation index (OSAVI)) for classifying forest successional stages and estimating AGB in eighteen permanent plots spanning Late-, Disturbed-, and Secondary Forest stages. Vegetation index values were extracted from six cloud-free Sentinel-2 images (cloud cover < 10%). Multinomial logistic regression and principal component analysis (PCA), combined with bootstrap resampling, were applied to classify forests by successional stage and biomass class and to predict plot-level AGB using field inventory data as reference. Classification accuracy for successional stages was high (90.3%), while accuracy for biomass classes was moderate (63.5%) and improved in the higher biomass class (~ 68%). Combined classification of successional stage and biomass class was less reliable (54.0%), likely reflecting high structural heterogeneity and overlap due to historical disturbance. The first principal component captured 93% of the variance in VI data but explained only 37% of the variation in AGB. These findings underscore the limitations of current VI approaches for precise AGB estimation in structurally complex tropical forests. Integrating additional remote sensing data and refined modeling techniques will be necessary to support more accurate forest conservation and management in the Atlantic Rainforest.

Keywords Remote sensing, Carbon, Forest inventory, Ecological succession, Atlantic Rainforest

1 Introduction

Tropical forests are central to the global carbon cycle and climate regulation because their biomass and soils store large quantities of carbon, buffering atmospheric CO_2 increases driven by fossil fuel combustion and land-use change such as deforestation and agriculture [27, 30, 31, 42, 45, 50]. In highly threatened biodiversity hotspots like the Atlantic Rainforest, where fragmentation and rapid loss of native cover intensify pressures on these carbon stocks and associated ecosystem services, precise mapping of forest disturbance and degradation becomes essential for effective conservation, climate mitigation, and the design of financial instruments such as carbon credits [26, 39, 53, 59, 70]. Within this context, satellite-derived vegetation indices (VIs) have become a primary tool for monitoring forest condition and disturbance dynamics, underpinning many REDD$^+$-type mechanisms and policies endorsed in international climate negotiations because they offer spatially explicit, repeatable measures of canopy status and productivity [36, 51]. However, optical VIs remains constrained by clouds, atmospheric effects, and saturation in high-biomass stands, limiting their capacity to detect subtle or understory disturbances and underscoring the need to better understand both their potential and limitations when used for disturbance mapping in complex tropical forest landscapes.

In this context, accurately quantifying biomass and indirectly estimating the carbon it stores becomes increasingly critical. Asner and Mascaro [5] outline several methods for assessing this reservoir, all of which rely on quantifying plant biomass, as approximately 48% of it is carbon in tropical forests. While forest inventory data provides estimates of aboveground biomass (AGB), significant gaps persist, particularly in Tropical Forest regions [64]. These challenges are especially acute in the Atlantic Rainforest, where field inventories are hampered by limited site access, severe landscape fragmentation, and the rapid pace of land use change [26, 53].

The implementation of continuous inventory programs offers a practical approach to assessing the magnitude of carbon exchange between ecosystems and the atmosphere [25]. Remote sensing techniques, when integrated with field measurements, can significantly enhance the precision and spatial extent of such assessments [23].

Remote sensing acquires information about Earth's surface features without physical contact, utilizing sensors that actively or passively record the interaction of electromagnetic radiation with the medium [60]. Some of these sensors operate within the optical portion of the electromagnetic spectrum, specifically in the visible, near-infrared, and shortwave-infrared ranges, relying on solar radiation reflected by target objects. This necessitates prior knowledge of their spectral signatures [60]. Vegetation indices (VIs), derived from mathematical transformations of original spectral reflectance data [49], are generated algorithmically from optical sensor images to facilitate the interpretation of vegetation cover and biomass. According to Kuntschik [37], image reflectance values must be converted to values of the desired vegetation index (VI) for each pixel. This transformation allows for the correlation of VI values with specific vegetation characteristics. The theoretical foundation of VIs is rooted in the contrast between high near-infrared reflectance and low red reflectance exhibited by vegetation [6].

As reviewed by Tian et al. [64], remote sensing products and their derived vegetation indices have frequently been used to estimate aboveground biomass in tropical forests, for example by integrating Sentinel-2 VIs with field data in Malaysian rainforests [1], combining Landsat-8 indices to model biomass in the Brazilian Caatinga [16], or relating Sentinel-2 NDVI, EVI and RVI to AGB in chir pine forests [2], and over the past decade Tian et al. [64] have highlighted that numerous studies have explored this application across a range of tropical forest ecosystems, integrating different methodologies, techniques, and modeling approaches.

Given the urgent need for precise, scalable methods to monitor forest biomass—particularly in response to ongoing deforestation and climate policies—this study evaluates the potential of satellite-based vegetation indices for aboveground biomass estimation in the highly fragmented Atlantic Rainforest. Our approach harnesses Sentinel-2 imagery to derive four widely used spectral indices (NDVI, EVI, RVI, and OSAVI), assessing their individual and combined performance across distinct stages of forest succession.

The main aims of this research are: (i) to rigorously assess how well these indices, both individually and as composite predictors, classify forest successional stages and predict biomass when compared to field inventory benchmarks; (ii) to explore modeling strategies that not only maximize predictive accuracy but also enhance interpretability and operational simplicity. In doing so, we address key methodological questions about index selection, model parsimony, and the integration of advanced analytical techniques. By directly comparing model outputs to ground-truth data and thoroughly analyzing the impacts of different predictor sets, this study provides critical insights into the practical strengths and current limitations of remote sensing for tropical forest biomass estimation. Ultimately, our findings are intended to guide future research efforts and inform the development of more robust, efficient, and accessible tools for forest monitoring and resource management in tropical landscapes.

2 Materials and methods

2.1 Study area

This study targeted areas measured in 2017 by Roder et al. [53], Guerrini et al. [26], and Sivisaca et al. [61] in the south-central region of São Paulo State, specifically in the municipality of Botucatu. The study sites were located within the Experimental Farms of the São Paulo State University (UNESP) and comprised fragments of Seasonal Semideciduous Forest.

The climate of the region is classified as humid subtropical (Cfa) according to the Köppen-Geiger climate classification system [3, 20]. Based on field data from the local station spanning the years 1997 to 2018, the average annual rainfall was 1494 mm, primarily concentrated between October and March. The average annual temperature for the same period is 20.5 °C, with monthly averages ranging from a minimum of 17.5 °C in July to a maximum of 23 °C in February [61].

The natural vegetation is classified as Tropical Semideciduous Seasonal Forest, a domain of the Atlantic Rainforest, with transitional fragments to *Cerradão* [34]. According to Nogueira Junior [46], some forest areas remain well-preserved, while others are undergoing natural regeneration. Based on vegetation successional stages, the fragments were categorized into three groups (Fig. 1).

The classification of forest patches into Late (LF), Disturbed (DF), and Secondary Forest (SF) followed a multi-criteria approach, building on detailed field inventories, local management records, historical aerial and satellite imagery, and site accessibility information [26, 53]. Specifically, succession stage categories were assigned based on features

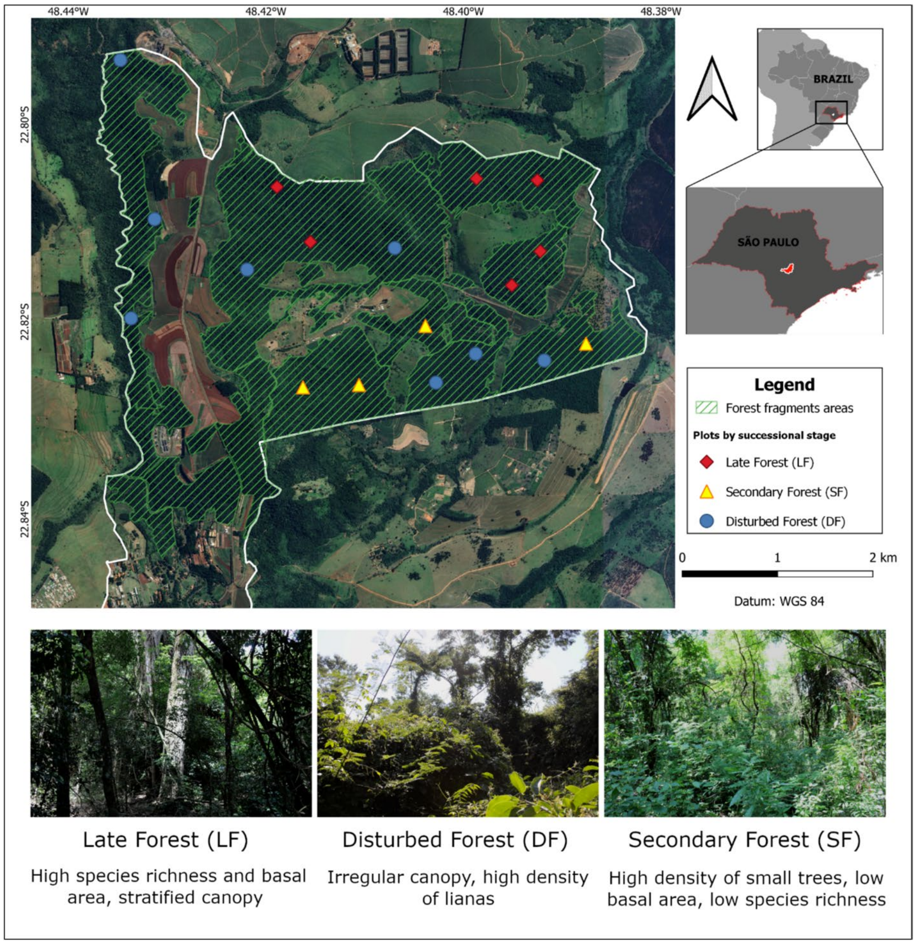

Fig. 1 Permanent plots location and their respective successional stage

reported in Table 1, thus reflecting a clear anthroposequence, ordered from lowest (LF) to highest (SF) human disturbance, and were established through a synthesis of physiognomic, floristic, and historical evidence for each fragment [26, 53].

Summarizing, the **late forest** (LF) (plots 1, 4, 12–15) exhibits mature native vegetation characterized by high species richness (> 100), a well-developed vertical structure, and significant biomass [26, 53, 61]. Its steep topography, resulting from a slope break in the *cuesta*, hinders accessibility and limited past exploration. The **disturbed forest** (DF), encompassing plots 2, 3, 7, 8, 10, 16–18, experienced significant disturbance from human activities, including selective logging and occasional fires from adjacent pastures, up until the 1970s [34]. Currently, it is in an intermediate stage of succession, with a notable abundance of lianas within the canopy. The **secondary forest** (SF), representative of plots 5, 6, 9, and 11, includes young or degraded secondary forests that regenerated following the abandonment of pastures since the 1980s [34]. These forests are characterized by a low, closed canopy, high density of slender trees, and reduced species richness (~ 80) [26, 53, 61].

In 2017, eighteen (18) randomly selected 20 m × 100 m (2000 m^2) permanent plot sampling units were established [26, 53, 61]. Field sampling was conducted using permanent plots distributed across the three forest successional stages. A total of eight plots were installed in Disturbed Forest, six plots in Late Forest, and four plots in Secondary Forest.

Table 1 Key features and criteria used to classify Atlantic Rainforest study fragments by successional stage (LF: Late Forest; DF: Disturbed Forest; SF: Secondary Forest)

Category	Years since major disturbance	Canopy/structure	Richness/composition	Accessibility
LF	> 40 years without intensive land use or logging before the investigation started (b.i.s)	Tall, closed, complex	High; late-successional species	Hardly accessible
DF	Selectively logged or burned up to 30–40 years b.i.s	Patchy, many lianas	Transitional; diverse/heterogeneous	Intermediate
SF	Converted to pasture and later abandoned, with succession beginning ~ 20 years b.i.s	Low, dense, simple	Lower; many pioneer/early species	More accessible

To minimize edge effects and other potential confounding factors, a minimum distance of 500 m was maintained between plots, and all plots were located at least 200 m from fragment boundaries. The forest fragments are situated within the geographic coordinates 22° 47′ 32″ S to 22° 50′ 08″ S latitude and 48° 22′ 54″ W to 48° 26′ 13″ W longitude. At that time, a comprehensive forest inventory was conducted to estimate biomass by measuring the height (H) and diameter at breast height (DBH) of all trees within each plot. Subsequently, allometric equations [14] were employed to calculate aboveground biomass.

2.2 Vegetation indices

To acquire and process satellite imagery, we used Google Earth Engine [24], a cloud-based geospatial analysis platform providing access to major remote sensing datasets (NASA, ESA, NOAA) with robust computational resources and scripting via JavaScript [63, 69]. We selected imagery from the MultiSpectral Instrument (MSI) on the ESA Sentinel-2 satellite, launched in 2015, which offers a spatial resolution of 10 m and a revisit interval of 5 days—both advantageous for monitoring fragmented landscapes compared to alternatives like Landsat 8. All subsequent analyses were anchored to permanent field plots established through forest inventory, which served as the ground reference for biomass and successional stage information.

Image acquisition was narrowly focused to coincide with the field measurements (September–November 2017; [26, 53, 61]) to ensure temporal correspondence between ground and remote observations. To guarantee image quality, we applied a cloud cover threshold of < 10%, selecting three optimal scenes (September 7, September 27, October 17, 2017). These acquisition dates were selected to ensure direct correspondence between satellite-derived vegetation indices and field-measured biomass values.

The subsequent JavaScript-based preprocessing, depicted in Fig. 2, involved: (i) satellite collection selection to identify relevant data sources; (ii) temporal matching of satellite scenes to exact field sampling dates; (iii) region of interest (ROI) definition to restrict analysis spatially; (iv) cloud masking using the selected threshold, and (v) temporal filtering to focus on the period in which field inventories were conducted.

By incorporating both strict spatial and temporal alignment, plus cloud filtering, we significantly improved dataset reliability for analysis.

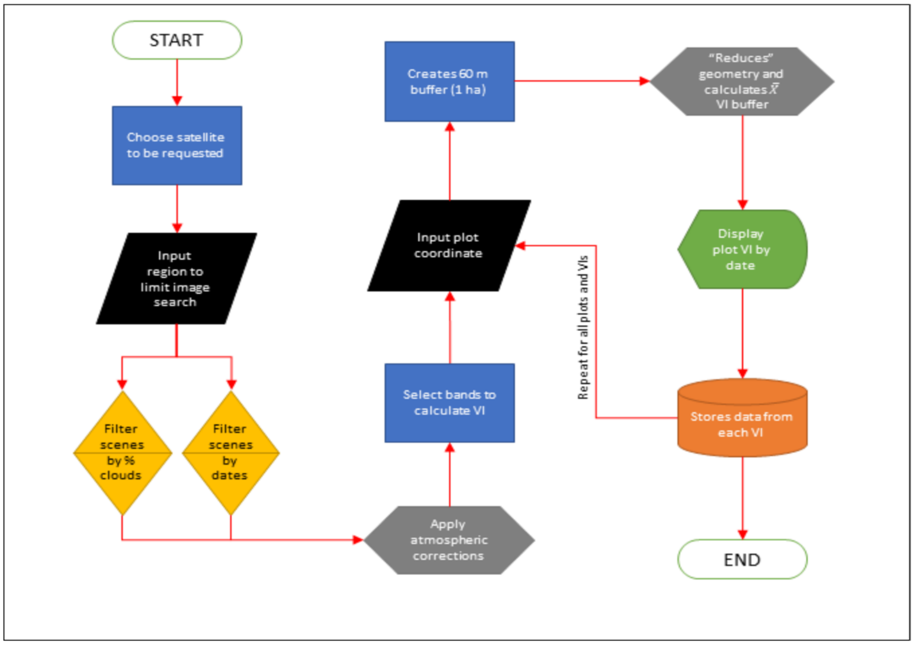

Fig. 2 Flowchart illustrating the workflow for scripting remote sensing data acquisition and vegetation Index (VI) elaboration

Table 2 Equations of the vegetation indices used

Vegetation index	Equation	References
Normalized difference vegetation index (NDVI)	$\mathrm{NDVI} = \frac{(NIR-R)}{(NIR+R)}$	Johnson and Wichern [32]
Enhanced vegetation index (EVI)	$\mathrm{EVI} = 2.5 \times \frac{(NIR-R)}{(NIR+6R-7.5B+1)}$	Diggle [14]
Ratio vegetation index (RVI)	$\mathrm{RVI} = \frac{NIR}{R}$	[21]
Optimized soil adjusted vegetation index (OSAVI)	$\mathrm{OSAVI} = \frac{(1+0.16)\times(NIR-R)}{(NIR+R+0.16)}$	[54]

NIR = near infrared, R = red, B = blue.

Prior to vegetation index (VI) calculation, atmospheric corrections must be applied to the satellite images. These images, obtained from the Engine platform, are delivered in top-of-atmosphere (TOA) reflectance. To address atmospheric distortions caused by aerosols and water vapor, the Sensor Invariant Atmospheric Correction (SIAC) method, proposed by Yin et al. [71], was employed to convert the TOA reflectance to surface reflectance.

Three spectral bands were utilized to compute the VIs (Table 2): near-infrared (B8), red (B4), and blue (B2). The algorithm subsequently applies the respective VI formulas to the corrected imagery, generating a new image where each pixel is assigned a VI value. To extract these values in a usable format, a 60-m buffer encompassing approximately one hectare is delineated around each plot. A reduction function is then applied to the buffer area, yielding the average pixel value for each permanent plot. These plot-level VI values were then directly linked to aboveground biomass estimates derived from field measurements and constituted the modeling samples used in all classification analyses. This averaged value is subsequently compared to the ground truth measurements obtained by Sivisaca et al., [61]. This process is repeated for each image, permanent plot, and all four indices.

2.3 Statistical analysis

2.3.1 Classification of forest fragments

Initially, for each forest fragment, a bootstrap simulation was employed to generate 1,000 random samples with replacement. To ensure reproducibility, a fixed random seed was set during all bootstrap resampling procedures. Field plots were subdivided into ten subplots each, which constituted the effective sampling units used in the statistical analyses. These samples were partitioned into modeling (60%) and validation (40%) subsets. The modeling sample sizes for disturbed, secondary, and late-successional fragments were 48, 24, and 36, respectively, while the validation samples were 32, 16, and 24. The *surveyselect* procedure in SAS [58] was used to implement this sampling strategy.

For each of 1000 iterations, a multinomial logistic regression model was fitted to classify forest fragments into three categories (disturbed, secondary, and late), using the four vegetation indices (NDVI, EVI, RVI, and OSAVI) as predictor variables. Analysis was performed with the GLIMMIX (generalized linear mixed models) procedure and *generalized logit* link [56]. Classification accuracy was assessed using the independent validation subsets (40% of the data) in each bootstrap iteration by comparing observed and predicted classes, ensuring robust, cross-validated estimates across the full simulation.

2.3.2 Classification of biomass

The biomass data from all three forest fragments were pooled and divided into two categories using the median biomass value of 140.32 Mg ha^{-1} as a threshold. This approach was adopted to evaluate whether spectral vegetation indices are capable of discriminating broad biomass classes independently of forest successional status, while ensuring balanced group sizes and adequate statistical power. The use of the median facilitated balanced group sizes, optimizing statistical power for the classification analysis. Category 1 encompassed values ranging from 13.35 to 140.32 Mg ha^{-1}, while category 2 included values from 140.32 to 795.51 Mg ha^{-1}.

After initial categorization, a bootstrap resampling technique was utilized to create 1,000 random subsets from the original dataset. Each subset was divided into training (60%) and validation (40%) sets, containing 162 and 108 observations, respectively. This resampling strategy allowed the robustness of biomass class discrimination to be evaluated across repeated realizations of the data.

For each of the 1000 repetitions, linear discriminant analysis (LDA) was applied in combination with a non-parametric k-nearest neighbor (KNN) classifier ($k = 4$) to account for potential non-linear separability and departures from normality in biomass-related spectral responses. This analysis was implemented using the SAS *discrim* procedure (*method* = *npar*, *crossvalidate*, $k = 4$ options), and accuracy was assessed using the respective validation sets.

2.3.2.1 Joint classification of biomass and forest fragments To better reflect the combined influence of forest structure and successional history on biomass distribution, the biomass within each forest fragment category was split into two classes, using the group-specific median as the threshold (*i.e.*, “low” and “high” biomass per fragment type).

Across the three forest types, this approach yielded a total of six unique forest–biomass classes for the joint classification analysis. These were:

a. Disturbed Forest: 31–106 Mg ha^{-1} and 106–796 Mg ha^{-1}
b. Secondary Forest: 20–140 Mg ha^{-1} and 140–340 Mg ha^{-1}
c. Late Forest: 13–254 Mg ha^{-1} and 254–730 Mg ha^{-1}

This joint stratification was designed to assess whether incorporating successional context improves biomass discrimination relative to biomass-only classification, particularly given the heterogeneity typical of tropical forest systems.

Following categorization, a bootstrap simulation was employed to generate 1,000 random samples for model training and validation. Each sample was divided into training and validation sets, with 60% and 40% of the data, respectively. For the disturbed forest, the training and validation set sizes were 72 and 48, respectively. For the secondary forest, these sizes were 36 and 24, respectively. Finally, for the late forest, the sizes were 54 and 36, respectively.

For the joint classification of forest fragments and biomass categories, we employed LDA combined with a non-parametric KNN classifier (k = 4). This was always implemented in SAS using the *discrim* procedure, specifying *method = npar*, *crossvalidate*, and *k* = 4, for each of the 1,000 bootstrap repetitions. To support full reproducibility and comparability, random number seeds and consistent split strategies were used across all iterations. For each bootstrapped sample, model accuracy was systematically assessed using the withheld validation subsets.

The rationale and sequence of all classification approaches (successional stage, biomass-only, and joint classification) are summarized schematically in Fig. 3, highlighting their complementary roles within the overall analytical framework.

2.3.3 Prediction of biomass

2.3.3.1 Principal components analysis (PCA) for the vegetation index: Principal component analysis (PCA) was applied to four vegetation indices (NDVI, EVI, RVI, and OSAVI). It constructs linear combinations of these indices, yielding new uncorrelated variables (principal components) that maximize variance. According to the Kaiser criterion [32], only principal components (PCs) with eigenvalues greater than one should be retained,here, only PC1 (eigenvalue = 3.76; PC2: eigenvalue = 0.20) met this criterion. However, the first two components together explained over 99% of the total variance and were then examined to assess whether any additional, interpretable spectral variation existed beyond the dominant component [32]. The *princom* procedure in SAS was employed for the analysis [57].

2.3.3.2 Generalized linear regression models incorporating repeated measures: Generalized linear regression models with gamma distribution and log-link function were fitted to the average biomass of each forest fragment, using the first principal component as a continuous covariate.

The biomass response variable, consisting of repeated measurements of four Sentinel-2 vegetation indices per plot over time, was analyzed using Generalized Estimating Equations (GEE) [14]. Model fit and adequacy were assessed using the *genmod* procedure in SAS, specifying a repeated subject structure for each plot. Diagnostic checks included deviance analysis and inspection of standardized Pearson residual plots to

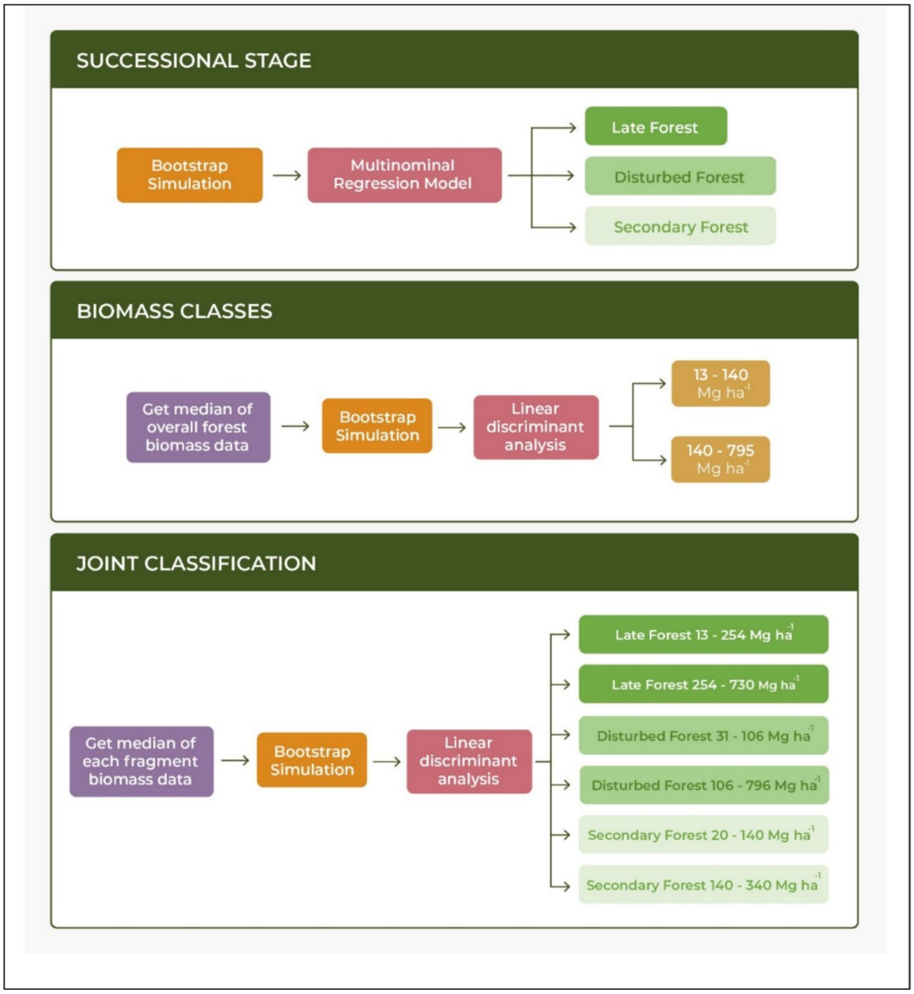

Fig. 3 Statistical flowchart for classification of the forest successional stages, biomass classes and joint classification

ensure that model assumptions were appropriately met. A comprehensive flowchart of these procedures is shown in Fig. 4.

3 Results

3.1 Classification of forest fragments and biomass

Table 3 presents the cross-validation results for the classification of forest fragments. The mean overall accuracy from 1000 bootstrap simulations was 90.27% (median = 89.82%; range = 83.33–99.07%), with a low coefficient of variation (3.07%), indicating high model stability. Late-successional fragments (LF) were most accurately classified, followed by DF and SF categories.

Table 4 presents the cross-validation results for the classification of two biomass categories (Mg ha^{-1}) using LDA with KNN (k = 4). The overall average accuracy of 63.50% was notably lower than that achieved in previous fragment classifications. Nevertheless, multinomial logistic regression models demonstrated partial suitability for identifying these categories based on the four spectral indices. Notably, the classification accuracy for the higher biomass class (140.32–795.50 Mg ha^{-1}) was 33.81%, significantly lower than that for the first category. The accuracy rate histogram exhibited low variability, with a coefficient of variation of 4.66% and a range of 52.78–73.78%.

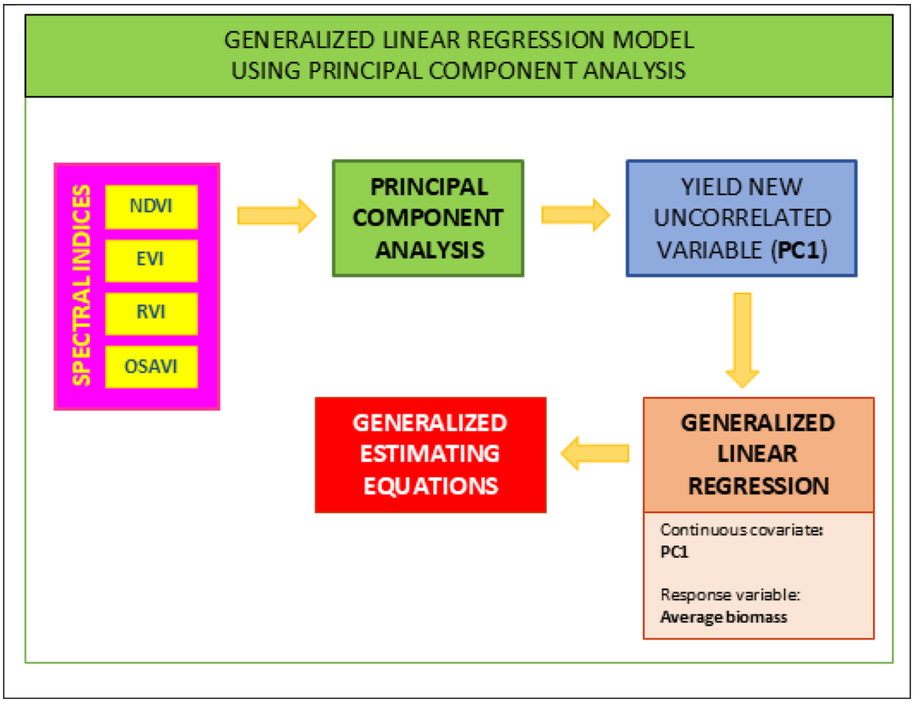

Fig. 4 Statistical flowchart of biomass prediction analysis

Table 3 Cross-validation confusion matrix and summary statistics from multinomial logistic regression (*glogit*) classifying forest fragments using Sentinel-2 indices (NDVI, EVI, RVI, OSAVI) over 1000 bootstrap simulations

Forest stage	Classification				Summary of accuracy rate of statistical simulation
	Disturbed	Secondary	Late	Total	
Disturbed	43,185 (39.99%)	4,815 (4.46%)	0 (0.00%)	48,000 (44.44%)	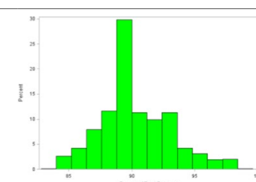
Secondary	5,699 (5.28%)	18,301 (16.95%)	0 (0.00%)	24,000 (22.22%)	
Late	0 (0.00%)	0 (0.00%)	36,000 (33.33%)	36,000 (33.33%)	
Total	48,884 (45.26%)	23,116 (21.40%)	36,000 (33.33%)	108,000 (100%)	
Accuracy rate = 100 (43,185 + 18,301 + 36,000)/108,000 = 90.27%					n = 1,000; mean = 90.27%; median = 89.82%; min = 83.33%; max = 99.07%; std.dev = 2.77%; coef. var. = 3.07%

3.2 Joint classification of forest fragments and biomass

Table 5 summarizes the accuracy rates for joint classification of forest fragments and biomass categories, where each fragment type's biomass was divided by the group's median value (for a total of six groups). The mean accuracy rate drops to 54.08%, considerably lower than that observed in previous classifications of fragments and biomass categories separately. This finding suggests that multinomial logistic regression models are not well-suited for this joint classification task. Additionally, the accuracy rate

Table 4 Cross-validation of biomass category classification for Sentinel-2 satellite using linear discriminant function with classification criterion considering the non-parametric distribution of data through the method of four nearest neighbors (KNN) for the three forest fragments (SF, DF, and LF)

	Classification			**Summary of accuracy rate of statistical simulation**
Biomass category	13.36⊢140.32	140.32⊢795.50	Total	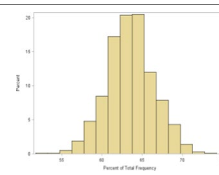
13.36⊢140.32	56,671 (29.65%)	40,246 (21.06%)	96,917 (50.70%)	
140.32⊢795.50	29,604 (15.49%)	64,619 (33.81%)	94,223 (49.30%)	
Total	86,275 (33.70%)	104,865 (33.11%)	191,140 (100%)	
Accuracy rate = 100(56,671 + 64,619)/191,140 = 63.46%				n = 1,000; mean = 63.50%; median = 63.43%; min = 52.78%; max = 73.78%; std. dev = 2.96%; oef. var. = 4.66%

Bootstrap simulation (n = 1000) was performed, considering the input variables NDVI, EVI, RVI, and OSAVI —summary of accuracy rate of statistical simulation

Table 5 Cross-validation of biomass category classification within each forest fragment, using the non-parametric distribution of data through the method of the four nearest neighbors, obtained through bootstrap simulation (n = 1000), considering the input variables as the NDVI, EVI, RVI, and OSAVI indices from the Sentinel-2 satellite

Classification							
Forest and biomass	**Disturbed**	**Disturbed**	**Secondary**	**Secondary**	**Late**	**Late**	**Total**
Categories	31–106	106–796	20–140	140–340	13–254	254–730	
Disturbed 31–106	21,759	18,723	138	289	143	758	41,810
	11.91	10.24	0.24	0.16	0.08	0.41	22.88
Disturbed 106–796	12,906	25,965	220	432	202	943	40,668
	7.06	14.21	0.12	0.24	0.11	0.52	22.25
Secondary 20–140	65	174	10,387	10,107	348	94	21,175
	0.04	0.10	5.68	5.53	0.19	0.05	11.59
Secondary 140–340	157	248	6,771	11,696	350	120	19,342
	0.09	0.14	3.70	6.40	0.19	0.07	10.58
Late 13–254	108	282	226	565	14,658	14,068	29,907
	0.06	0.15	0.12	0.31	8.02	7.70	16.36
Late	191	432	155	346	14,363	14,367	29,854
254–730	0.10	0.24	0.08	0.19	7.86	7.86	16.34
Total	35,186	45,824	17,897	23,435	30,064	30,350	182,756
	19.25	25.07	9.79	12.82	16.45	16.61	100

Accuracy Rate = 100(21,759 + 25,965 + 10,387 + 11,696 + 14,658 + 14,367) / 182,756 = 54.08%

Summary of accuracy rate of statistical simulation: n = 1,000; mean = 54.14%; median = 63.43%; min = 42.63%; max = 64.23%; std.dev = 3.54%; coef. var. = 6.54%

histogram exhibits low variability, with a coefficient of variation of 6.54% and a range of 42.63–64.23%.

3.3 Biomass prediction

In this section, we will explore the potential of modeling biomass using four spectral indices. While individual or combined regression models based on these indices yielded unsatisfactory results, we opted to initially extract the first principal component and subsequently refine our regression models.

Table 6 Eigenvalues of the correlation matrix for the first two principal components of four Sentinel-2 spectral indices (NDVI, EVI, RVI, and OSAVI)

Components	Eigenvalue	Proportion (%)	Cumulative proportion (%)
PC1	3.759	93.98	93.98
PC2	0.204	0.0511	99.09

Eigenvectors:

PC1 = 0.4965(NDVI) + 0.4909(EVI) + 0.5014(RVI) + 0.5110(OSAVI)
PC2 = − 0.5414(NDVI) + 0.6772(EVI) − 0.4121(RVI) + 0.2800(OSAVI).

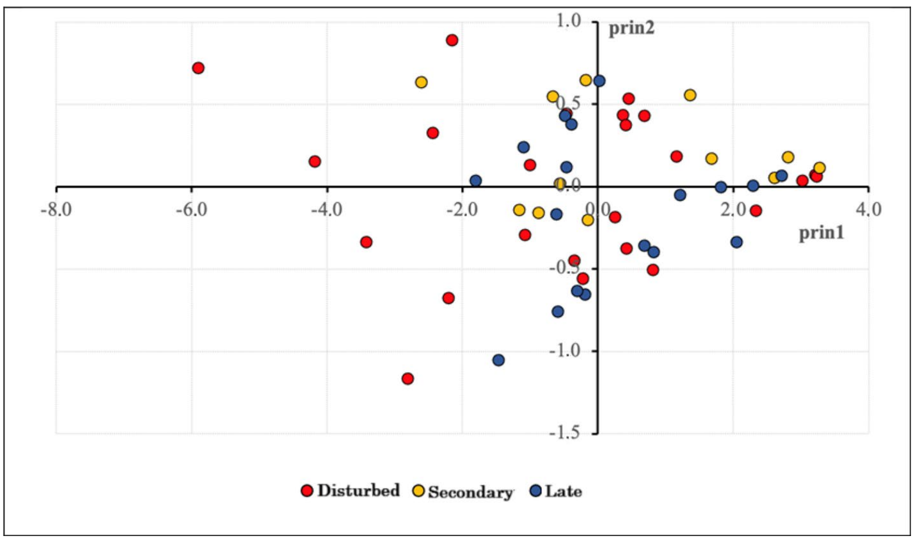

Fig. 5 The first and second principal components (PC1 and PC2) for the four spectral indices (NDVI, EVI, RVI, and OSAVI) of the Sentinel-2 satellite according to fragments

3.3.1 Principal components analysis for the vegetation index

Table 6 displays the eigenvalues and eigenvectors of the correlation matrix for the first two principal components derived from four spectral indices (NDVI, EVI, RVI, and OSAVI) obtained from Sentinel-2 satellite imagery. The first principal component (PC1) accounts for 93.98% of the total variance (eigenvalue = 3.759) and effectively summarizes the main spectral variability. PC1 was thus used as a continuous predictor in subsequent regression analyses (Fig. 5) to predict biomass (Mg ha^{-1}).

3.3.2 Generalized regression models with repeated measures approach

Table 7 presents the results of a generalized linear mixed model (GLMM) with a gamma distribution, log link function, and a repeated measures structure, fitted using GEE. The model's parameter estimates, $\widehat{\beta}_0$ and $\widehat{\beta}_1$, were found to be statistically significant ($p < 0.05$), indicating a significant regression relationship. Model diagnostics—including deviance analysis and standardized Pearson r esiduals within the interval [− 2, 2]—confirmed that model assumptions were met.

However, the empirical R^2 was notably low, suggesting that while a significant relationship exists, much of the biomass variability remains unexplained by the spectral indices alone. Furthermore, model fit for secondary (SF) and late-successional fragments (LF) was poor and not further analyzed here, highlighting the challenge of predicting biomass in structurally complex and heterogeneous forest conditions.

Table 7 Generalized linear regression results (gamma GLMM, repeated measures structure, GEE) for biomass prediction using PC1 from Sentinel-2 indices

Model adjusted for biomass (Y) as a function of prin1, estimated parameters followed by p-values in parentheses, empirical determination coefficients

$\widehat{Y} = exp\left(\widehat{\beta}_0 + \widehat{\beta}_1\,(prin1)\right);$

$\widehat{\beta}_0 = 5.0060\,(< 0.0001)\,;$

$\widehat{\beta}_1 = -0.0647\,(0.0479)\,;$

$R_e^2 = 37.47\%$

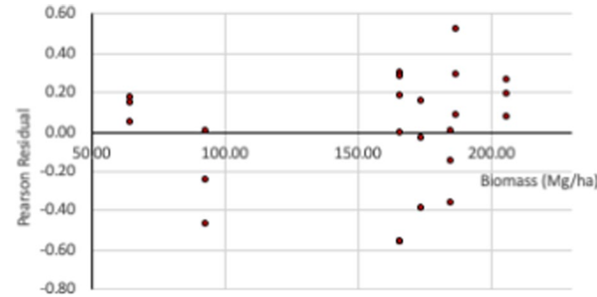

$prin1 = 0.4965\,(NDVI) + 0.4909\,(EVI) + 0.5014\,(RVI) + 0.5110\,(OSAVI)$

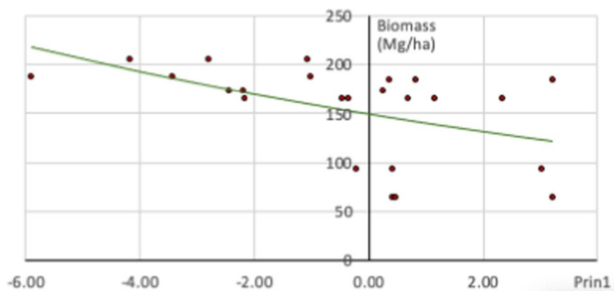

[1] (*) Square of the Spearman correlation coefficient between estimated and observed values. The employed modelized the average biomass (Ŷ) as a function of the first principal component (Prin1) derived from four spectral indices (NDVI, EVI, RVI, and OSAVI). Estimated parameters, empirical coefficient of determination (R^2), degrees of freedom-adjusted deviances, and residuals were calculated for the disturbed forest fragments

4 Discussion

4.1 Classification of forest fragments

The observed overall average accuracy (90.27%) suggests that multinomial logistic regression models are suitable for identifying the three forest fragments studied, based on the four spectral indices considered. Furthermore, the low variability of the accuracy rate histogram supports this conclusion. To classify forest fragments into three successional stages (Late-, Secondary-, and Disturbed Forest), as previously identified by previous studies [26, 53, 61] through forest inventory data analysis, four vegetation indices (NDVI, EVI, RVI, and OSAVI) were employed. A multinomial logistic regression model achieved a high average classification accuracy of 90.27% with a low coefficient of variation (3.07%), indicating strong performance. This result is consistent with findings from Garroutte et al. [21], who used polynomial-adjusted models with NDVI and EVI to map grassland quality in Yellowstone. The strong discriminatory power of these indices is likely due to marked differences in canopy structure, species composition, and disturbance history among successional stages, which are well captured by spectral signals in both the red and near-infrared bands [10, 68].

The effectiveness of vegetation indices in assessing temporal variations in forest conditions is well-established. Numerous studies have demonstrated their utility in forest monitoring, particularly during regeneration and disturbance phases [11, 54, 67]. These methods provide valuable insights for forest restoration and conservation efforts, enabling large-scale interventions with reduced costs and time [9, 15]. However, the broad application of remote sensing is limited by site-specific factors, such as the complex canopy structure of tropical forests, which can influence canopy reflectance [62]. While our accuracy mirrors that observed in more structurally simplified systems, caution is warranted when extrapolating to regions with extreme canopy complexity, nonlinear successional pathways, or frequent edge effects, where classification performance may decline due to mixed spectral signatures [65]

Collectively, these findings reaffirm the strong potential of remote sensing for rapid, landscape-scale ecological monitoring in tropical forest mosaics, while underscoring the critical need for approaches that account for site-specific canopy structure and successional dynamics. Effectively harnessing these technologies will depend not only on their ability to detect broad ecological patterns, but also on an in-depth understanding of the unique structural and compositional attributes that shape each forest fragment's spectral signature.

4.2 Classification of biomass

A more challenging task proved to be the classification of forests by biomass categories. Our results yielded a moderate classification accuracy of 63.5%, likely hindered by the high variability in forest composition across tropical regions, which can complicate satellite sensor readings. Nevertheless, a slightly higher accuracy of approximately 68% was observed for the largest biomass class, potentially attributable to the larger trees with more expansive crown areas, leading to increased overall canopy reflectance. Additionally, the uneven spatial distribution of large trees in fragmented landscapes introduces further variability, which can dampen the discriminating ability of conventional vegetation indices [38]. This performance, however, falls slightly short of the accuracy reported by Dimitrov and Roumenina [15] in Bulgaria and Devagiri et al. [13] in India. This lower accuracy for high-biomass classes may reflect greater structural heterogeneity, the saturation effect of vegetation indices at higher biomass, and the presence of complex canopy layers or emergent species that are not fully distinguishable with optical data alone [44]. Ultimately, this highlights the persistent challenges of quantifying forest function from space in highly heterogeneous tropical mosaics, especially as biomass increases.

The integration of remote sensing techniques with field surveys is rapidly expanding, enhancing the accuracy and efficiency of forest inventories and related planning activities. Applications include forest stratification, sample plot allocation [13], biomass classification [12], and the assessment of wildfire-affected areas [18]. Advances in machine learning, such as the use of the Random Forest algorithm by Dube and Mutanga [17] for biomass classification, and Ma et al. [41], who incorporated additional spectral bands and vegetation indices, have further improved the accuracy of forest volume estimation, achieving levels as high as 80% [22].

Ultimately, our biomass classification results illustrate both the promise and persistent challenges facing efforts to derive functional ecosystem properties from optical satellite data in highly heterogeneous tropical regions.

4.3 Joint classification of forest fragments and biomass

The joint classification, designed to predict biomass class within each conservational status, achieved significantly lower accuracy (54%) compared to individual predictions of biomass or forest status. This compounded task proved challenging because it requires the model to resolve both floristic succession and subtle biomass gradients simultaneously, amplifying the confounding effects of historical fragmentation, canopy gaps, and overlapping species assemblages [47]. The model struggled to accurately classify biomass within specific conservational trajectories, as evidenced by a high coefficient of variation (>6%). This inefficiency may be attributed to the high spatial heterogeneity of the seasonal forest. The natural incidence of light and subsequent proliferation of lianas in these forests, particularly in disturbed areas, leads to increased variability in spectral signatures. Even in late-successional (LF) and secondary forests (SF), gaps with lower vegetation and higher liana and bamboo density can disrupt the joint classification of forest status and biomass class. Additionally, spectral confusion between edge and interior plots, as well as the coexistence of early- and late-successional traits within single fragments, further complicated accurate discrimination.

A significant challenge in joint classification arises from the similarity in aboveground biomass between DF and SF, both estimated to be around 120–180 Mg ha^{-1} [35]. However, their distinct disturbance histories lead to substantial variability in spectral signatures. While the DF experienced selective logging until the early 1980s and occasional fires, it has remained relatively undisturbed since then. Conversely, SF underwent deforestation for agriculture and pasture, followed by natural regeneration since the 1980s. These contrasting histories result in differences in structure and species composition, making it difficult to differentiate between the two forest types using remote sensing [4].

The inaccuracy of joint classification using satellite imagery underscores the potential of artificial intelligence tools to enhance the precision of biomass prediction from remote sensing data [40]. Artificial intelligence could be particularly valuable in joint classification for identifying current forest structure and species composition patterns influenced by past events, such as disturbances. This could improve biomass prediction within specific historical trajectories of forest fragments, as demonstrated by the success of multinomial logistic regression in predicting current forest status.

More precise remote sensing techniques, such as LiDAR [7, 52], could significantly enhance biomass prediction within different forest statuses. However, its application, especially in smaller areas, remains cost-prohibitive, necessitating careful cost–benefit analyses [8]. Nevertheless, recent advancements in artificial intelligence offer potential to increase the affordability and efficiency of LiDAR and other remote sensing tools [55].

These joint classification outcomes underscore how ecological complexity—created by mixed disturbance histories and succession pathways—can limit the precision of even advanced remote sensing models, emphasizing the evolving frontier of predictive forest ecology.

4.4 Biomass prediction by model fitting using PCA components

Principal Component Analysis (PCA) is a powerful dimensionality reduction technique that preserves the maximum variance of a dataset. In this study, the first principal component (PC1) accounted for over 93% of the total variation, making it an efficient summary variable and a suitable input for a forest biomass predictive model based on spectral indices. By combining four vegetation indices (NDVI, EVI, RVI, and OSAVI) into a single principal component, we streamlined the model, mitigated multicollinearity among predictors, and improved interpretability by simplifying the analysis of relationships [33].

However, the relatively low R^2 value (37%) suggests that PC1 alone is insufficient to explain the variability in biomass prediction fully. This finding aligns with prior work indicating that, in dense tropical forests, spectral indices often reach a saturation point and lose sensitivity to further increases in biomass [5, 6]. This limitation may be attributed to challenges encountered in earlier classification models, including the high heterogeneity in the structure and canopy cover of seasonal tropical forests, as well as significant species diversity, which contributes to highly variable biomass across the area [43]. Additionally, factors such as soil fertility, known to influence biomass [66], were not incorporated into the model. The low explanatory power indicates that incorporating additional covariates or interactions may be necessary to enhance model performance [29]. Furthermore, misalignment between field plot size and satellite pixel resolution may have contributed to unexplained variance, especially in small or heterogeneous patches [48].

Future research should focus on refining predictive models by optimizing vegetation index selection and testing various combinations of these indices, as a more parsimonious selection or combination might enhance model performance [43]. In addition, incorporating further covariates—such as soil moisture, canopy cover, or microclimate data—could directly influence biomass accumulation and improve predictive capability [48]. The integration of advanced remote sensing technologies, including LiDAR [64] and multi-sensor data [72], may yield higher spatial and vertical resolution, resulting in more accurate biomass estimates and better support for forest management and conservation efforts [19, 28].

In summary, while dimensionality reduction improves model simplicity, fully capturing the ecological variability of tropical forests will require both richer input data and more nuanced modeling approaches.

5 Implications for forest management

The outcomes of this study provide actionable insights for forest ecologists and managers tasked with navigating the challenges of highly fragmented tropical landscapes. The demonstrated high accuracy in classifying successional stages using Sentinel-2 vegetation indices underscores the practicality of rapid, cost-effective landscape assessments—an approach especially valuable for prioritizing restoration sites, monitoring natural regeneration, and identifying areas impacted by recent disturbances. These functions address core management needs and can be achieved with limited budgets and staff, making them highly scalable for conservation projects.

The moderate accuracy achieved for biomass class prediction indicates that, while current approaches are suitable for generating preliminary carbon stock estimates and informing carbon credit initiatives, they are best used for broad ecosystem service valuations rather than detailed, plot-level assessments. In particular, these spectral methods can support project planning and verification in settings where field inventories are limited or infeasible.

At the same time, the limitations revealed here should guide practitioners in adapting expectations and strategies. While spectral indices effectively capture vegetation recovery and successional transitions, they may miss finer-scale variability in biomass, particularly in structurally complex or historically disturbed stands. To address this, managers can use remote sensing to direct ground surveys to areas of greatest spectral uncertainty or change, efficiently allocating effort and resources. Additionally, the consolidation of multiple indices through principal component analysis presents a route to streamline operational workflows and reduce data complexity.

Collectively, these findings support the integration of remote sensing tools into everyday management and policy frameworks, maximizing impact while minimizing costs. However, for applications requiring high precision—such as carbon accounting or high-resolution habitat mapping—there remains a clear need to supplement spectral approaches with next-generation technologies like LiDAR and multi-sensor data fusion. By matching methods to management needs and resource constraints, practitioners can robustly leverage these evolving tools for more effective tropical forest conservation.

6 Conclusions

The obtained research's outcomes show that satellite-based vegetation indices, if applied with robust statistical models, can accurately distinguish successional stages in the highly fragmented Atlantic Rainforest, thus offering a possible efficient tool for broad-scale environmental monitoring. However, it is important to underline that predicting aboveground biomass remains a notable challenge if using spectral indices only, as clearly evidenced by the moderate classification accuracy and limited predictive power after data reduction. Such limitations highlight (*i*) the complexity and (*ii*) structural variability featuring the tropical forests, an environment where historical disturbance and species heterogeneity constrain the effectiveness of current remote sensing approaches. While streamlined techniques such as PCA help summarize spectral information, further progress will depend on the integration of additional environmental variables and advanced remote sensing technologies—especially LiDAR and multi-sensor data—to capture finer details of forest structure and function. As a matter of fact, a continued refinement of biomass modeling is pivotal for supporting carbon accounting, conservation prioritization, and adaptive management in tropical forest regions. This is particularly true for fragmented human-disturbed areas. As data availability and technological accessibility advance, these approaches have the potential to become indispensable components of effective, scalable forest resource management.

Acknowledgements
The authors would like to thank the Teaching, Research and Extension Farm (FEPE-UNESP/Botucatu) for their invaluable logistical assistance during the field phase. We also thanks to Coordenação de Aperfeiçoamento de Pessoal de Nivel Superior (CAPES-PrInt Program), Brasil [Grant Number: 88887.194785/2018-00, 2018] and CNPq-National Council for Scientific and Technological Development [Grant Numbers: 308916/2017-4, 2017; 311623/2020-4, 2020].

Author contributions
During the writing process, the corresponding author utilized the Grammarly tool to enhance the consistency of language across authors coming from different countries. At the end of the final version, all the authors have reviewed and edited the content. Finally, a native English speaker did the final language editing. All authors take full responsibility for the content of the publication. The authors declare no conflict of interest.

Data availability
All raw data can be provided by the corresponding author upon request.

Declarations

Ethics approval and consent to participate
Not applicable.

Consent for publication
Not applicable.

Competing interests
The authors declare no competing interests.

Received: 28 October 2025 / Accepted: 4 May 2026

Published online: 24 May 2026

References

1. Adan MS. Integrating sentinel-2 derived vegetation indices and terrestrial laser scanner to estimate above-ground biomass/carbon in Ayer Hitam tropical forest Malaysia. Master's thesis. University of Twente, Twente. 2017.
2. Ali N, Saad M, Anwar A, Ahmad N, Khan IA, Ullah H, et al. Assessment of aboveground biomass and carbon stock of subtropical pine forest of Pakistan. J For Sci. 2023;69(7):287. https://doi.org/10.17221/125/2022-JFS.
3. Alvares CA, Stape JL, Sentelhas PC, De Moraes Gonçalves JL, Sparovek G. Köppen's climate classification map for Brazil. Meteorol Z. 2013;22:711–28. https://doi.org/10.1127/0941-2948/2013/0507.
4. Arcanjo FA, Barufi GM, Torezan JMD. Selective logging that occurred decades ago is still impacting aboveground biomass and tree assemblage structure in Brazilian semi-deciduous seasonal Atlantic forest fragments. For Ecol Manage. 2023;535:120895. https://doi.org/10.1016/j.foreco.2023.120895.
5. Asner GP, Mascaro J. Mapping tropical forest carbon: calibrating plot estimates to a simple LiDAR metric. Remote Sens Environ. 2014;140:614–24. https://doi.org/10.1016/j.rse.2013.09.023.
6. Baret F, Guyot G. Potentials and limits of vegetation indices for LAI and APAR assessment. Remote Sens Environ. 1991;35:161–73. https://doi.org/10.1016/0034-4257(91)90009-U.
7. Borsah AA, Nazeer M, Wong MS. LIDAR-based forest biomass remote sensing: a review of metrics, methods, and assessment criteria for the selection of allometric equations. Forests Basel. 2023;14:2095. https://doi.org/10.3390/f14102095.
8. Bush G, Taye FA, Fleming C, Samndong RA. Evaluating the costs of primary forest conservation in the Democratic Republic of Congo, implications for policy and practice. J Environ Manage. 2024;352:119975. https://doi.org/10.1016/j.jenvman.2023.119975.
9. Cabral RP, Da Silva GF, De Almeida AQ, Bonilla-Bedoya S, Dias HM, De Mendonça AR, et al. Mapping of the successional stage of a secondary forest using point clouds derived from UAV photogrammetry. Remote Sens. 2023;15:509. https://doi.org/10.3390/rs15020509.
10. Cho MA, Sobhan I, Skidmore AK, de Leeuw J. Discriminating species using hyperspectral indices at leaf and canopy scales. Int Arch Photogramm Remote Sens Spat Inf Sci. 2008;XXXVII(B7):369–76.
11. Calvão T, Palmeirim JM. Mapping Mediterranean scrub with satellite imagery: biomass estimation and spectral behaviour. Int J Remote Sens. 2004;25:3113–26. https://doi.org/10.1080/01431160310001654978.
12. Clerici N, Rubiano K, Abd-Elrahman A, Posada Hoestettler J, Escobedo F. Estimating aboveground biomass and carbon stocks in periurban Andean secondary forests using very high resolution imagery. Forests Basel. 2016;7:138. https://doi.org/10.3390/f7070138.
13. Devagiri GM, Money S, Singh S, Dadhawal VK, Patil P, Khaple A, et al. Assessment of above ground biomass and carbon pool in different vegetation types of south western part of Karnataka, India using spectral modeling. Trop Ecol. 2013;54:149–65.
14. Diggle P. Analysis of longitudinal data. 2nd ed. Oxford Statist: Sci. Ser., Oxford Univ. Press, Oxford; 2013.
15. Dimitrov P, Roumenina E. Combining SPOT 5 imagery with plotwise and standwise forest data to estimate volume and biomass in mountainous coniferous site. Open Geosci. 2013. https://doi.org/10.2478/s13533-012-0124-9.

16. do Nascimento DM, Sales AT, Souza R, da Silva ASA, Sampaio EVDSB, Menezes RSC. Development of a methodological approach to estimate vegetation biomass using remote sensing in the Brazilian semiarid NE region. Remote Sens Appl Soc Environ. 2022;27:100771. https://doi.org/10.1016/j.rsase.2022.100771.
17. Dube T, Mutanga O. Evaluating the utility of the medium-spatial resolution Landsat 8 multispectral sensor in quantifying aboveground biomass in uMgeni catchment, South Africa. ISPRS J Photogramm Remote Sens. 2015;101:36–46. https://doi.org/10.1016/j.isprsjprs.2014.11.001.
18. Falkowski MJ, Gessler PE, Morgan P, Hudak AT, Smith AMS. Characterizing and mapping forest fire fuels using ASTER imagery and gradient modeling. For Ecol Manage. 2005;217:129–46. https://doi.org/10.1016/j.foreco.2005.06.013.
19. Fassnacht FE, White JC, Wulder MA, Næsset E, Achim A. Remote sensing in forestry: current challenges, considerations and directions. Forestry. 2024;97(1):11–37. https://doi.org/10.1093/forestry/cpad024.
20. Franco JR, Dal Pai E, Calça MVC, Raniero MR, Dal Pai A, Sarnighausen VCR, et al. Atualização da normal climatológica e classificação climática de Köppen para o município de Botucatu-SP. Irriga. 2023;28:77–92. https://doi.org/10.15809/irriga.2023v28n1p77-92.
21. Garroutte EL, Hansen AJ, Lawrence RL. Using NDVI and EVI to map spatiotemporal variation in the biomass and quality of forage for migratory elk in the Greater Yellowstone Ecosystem. Remote Sens. 2016;8:404. https://doi.org/10.3390/rs8050404.
22. Gerolamo CS, Pereira L, Costa FRC, Jansen S, Angyalossy V, Nogueira A. Lianas in tropical dry seasonal forests have a high hydraulic efficiency but not always a higher embolism resistance than lianas in rainforests. Ann Bot. 2024;134:337–50. https://doi.org/10.1093/aob/mcae077.
23. Goetz SJ, Dubayah R. Advances in remote sensing technology and implications for measuring and monitoring forest carbon stocks and change. Carbon Manag. 2011;2:231–44. https://doi.org/10.4155/cmt.11.18.
24. Gorelick N, Hancher M, Dixon M, Ilyushchenko S, Thau D, Moore R. Google earth engine: planetary-scale geospatial analysis for everyone. Remote Sens Environ. 2017;202:18–27. https://doi.org/10.1016/j.rse.2017.06.031.
25. Grace J. Understanding and managing the global carbon cycle. J Ecol. 2004;92:189–202. https://doi.org/10.1111/j.0022-0477.2004.00874.x.
26. Guerrini IA, da Silva JP, Lozano Sivisaca DC, et al. Evaluating carbon stocks in soils of fragmented Brazilian Atlantic Forests (BAF) based on soil features and different methodologies. Sci Rep. 2024;14:10007. https://doi.org/10.1038/s41598-024-60629-y.
27. Hansen J, Ruedy R, Sato M, Lo K. Global surface temperature change. Rev Geophys. 2010;48:RG4004. https://doi.org/10.1029/2010RG000345.
28. He J, Li W, Zhao Z, Zhu L, Du X, Xu Y, et al. Recent advances and challenges in monitoring and modeling of disturbances in tropical moist forests. Front Remote Sens. 2024;5:1332728. https://doi.org/10.3389/frsen.2024.1332728.
29. Huang T, Ou G, Wu Y, Zhang X, Liu Z, Xu H, et al. Estimating the aboveground biomass of various forest types with high heterogeneity at the provincial scale based on multi-source data. Remote Sens. 2023;15:3550. https://doi.org/10.3390/rs15143550.
30. IPCC. Climate change 2021: the physical science basis. contribution of working group I to the sixth assessment report of the intergovernmental panel on climate change. Cambridge: Cambridge Univ. Press; 2021.
31. James JN, Kates N, Kuhn CD, Littlefield CE, Miller CW, Bakker JD, et al. The effects of forest restoration on ecosystem carbon in western North America: a systematic review. For Ecol Manage. 2018;429:625–41. https://doi.org/10.1016/j.foreco.2018.07.029.
32. Johnson RA, Wichern DW. Applied multivariate statistical analysis. 6th ed. Upper Saddle River: Pearson/Prentice Hall; 2007.
33. Jolliffe IT, Cadima J. Principal component analysis: a review and recent developments. Philos Trans R Soc A Math Phys Eng Sci. 2016;374:20150202. https://doi.org/10.1098/rsta.2015.0202.
34. Jorge LAB, Sartori MS. Uso do solo e análise temporal da ocorrência de vegetação natural na Fazenda Experimental Edgardia, em Botucatu-SP. Rev Árvore. 2002;26:585–92. https://doi.org/10.1590/S0100-67622002000500009.
35. Justino STP. Dinâmica Florestal e Estoque de Carbono em Fragmentos de Mata Atlântica. MSc Thesis, Universidade Estadual Paulista, Botucatu. 2024.
36. Keith H, Vardon M, Stein JA, Lindenmayer D. Contribution of native forests to climate change mitigation–a common approach to carbon accounting that aligns results from environmental-economic accounting with rules for emissions reduction. Environ Sci Policy. 2019;93:189–99. https://doi.org/10.1016/j.envsci.2018.11.001.
37. Kuntschik G. Estimativa de Biomassa Vegetal Lenhosa em Cerrado por Meio de Sensoriamento Remoto Óptico e de Radar. MSc Thesis, Universidade de São Paulo, São Paulo. 2004.
38. López-Serrano PM, López-Sánchez CA, Díaz-Varela RA, Corral-Rivas JJ, Solís-Moreno R, Vargas-Larreta B, et al. Estimating biomass of mixed and uneven-aged forests using spectral data and a hybrid model combining regression trees and linear models. iForest. 2015;9:226–34. https://doi.org/10.3832/ifor1504-008.
39. Lovins LH, Cohen B. Climate capitalism: capitalism in the age of climate change. 1st ed. New York: Hill and Wang; 2011.
40. Luo M, Anees SA, Huang Q, Qin X, Qin Z, Fan J, et al. Improving forest above-ground biomass estimation by integrating individual machine learning models. Forests. 2024;15:975. https://doi.org/10.3390/f15060975.
41. Ma T, Hu Y, Wang J, Beckline M, Pang D, Chen L, et al. A novel vegetation index approach using Sentinel-2 data and random forest algorithm for estimating forest stock volume in the Helan Mountains, Ningxia, China. Remote Sens. 2023;15:1853. https://doi.org/10.3390/rs15071853.
42. Malhi Y, Silman M, Salinas N, Bush M, Meir P, Saatchi S. Introduction: elevation gradients in the tropics: laboratories for ecosystem ecology and global change research. Glob Change Biol. 2010;16:3171–5. https://doi.org/10.1111/j.1365-2486.2010.02323.x.
43. Merrick T, Pau S, Detto M, Broadbent EN, Bohlman SA, Still CJ, et al. Unveiling spatial and temporal heterogeneity of a tropical forest canopy using high-resolution NIRv, FCVI, and NIRvrad from UAS observations. Biogeosciences. 2021;18:6077–91. https://doi.org/10.5194/bg-18-6077-2021.
44. Mutanga O, Skidmore AK. Narrow band vegetation indices overcome the saturation problem in biomass estimation. Int J Remote Sens. 2004;25(19):3999–4014. https://doi.org/10.1080/01431160310001654923.
45. NOAA–National Oceanic & Atmospheric Administration, 2020. Trends in Atmospheric Carbon Dioxide (CO_2). Global Monitoring Laboratory, Boulder. https://gml.noaa.gov/ccgg/trends/ (Accessed 8 Aug 2025).

46. Nogueira LR. Estoque de Carbono na Fitomassa e Mudanças os Atributos dos Solos em Diferentes Modelos de Restauração de Mata Atlântica. MSc Thesis, Universidade de São Paulo, Piracicaba. 2010.
47. Nunes MH, Vaz MC, Camargo JLC, et al. Edge effects on tree architecture exacerbate biomass loss of fragmented Amazonian forests. Nat Commun. 2023;14:8129. https://doi.org/10.1038/s41467-023-44004-5.
48. Ordway EM, Asner GP, Burslem DFRP, Lewis SL, Nilus R, Martin RE, et al. Mapping tropical forest functional variation at satellite remote sensing resolutions depends on key traits. Commun Earth Environ. 2022;3:247. https://doi.org/10.1038/s43247-022-00564-w.
49. Patel NK, Saxena RK, Shiwalkar A. Study of fractional vegetation cover using high spectral resolution data. J Indian Soc Remote Sens. 2007;35:73–9. https://doi.org/10.1007/BF02991835.
50. Pierrehumbert R. Principles of planetary climate. Cambridge: Cambridge Univ. Press; 2010.
51. Rei FCF, Gonçalves AF, Souza LPD. Acordo de Paris: reflexões e desafios para o regime internacional de mudanças climáticas. Veredas do Direito: Direito Ambiental e Desenvolvimento Sustentável. 2017;14:81–99. https://doi.org/10.18623/rvd.v14i29.996.
52. Rodda SR, Fararoda R, Gopalakrishnan R, Jha N, Réjou-Méchain M, Couteron P, et al. LiDAR-based reference aboveground biomass maps for tropical forests of South Asia and Central Africa. Sci Data. 2024;11:334. https://doi.org/10.1038/s41597-024-03162-x.
53. Roder LR, Guerrini IA, Lozano Sivisaca DC, Yaguana Puglla CA, Góes de Moraes F, Pinheiro da Silva J, et al. Atlantic rainforest natural regeneration in fragmented formations affected by increasing human disturbance. J Environ Manage. 2023;1(325):116521. https://doi.org/10.1016/j.jenvman.2022.116521.
54. Rondeaux G, Steven M, Baret F. Optimization of soil-adjusted vegetation indices. Remote Sens Environ. 1996;55:95–107. https://doi.org/10.1016/0034-4257(95)00186-7.
55. Salehi-Dorcheabedi M, Asgari J, Amiri-Simkooei A, Fatemi Nasrabadi SB. Improving LiDAR height precision in urban environment: low-cost GNSS ranging prototype for post-mission airborne laser scanning enhancement. Remote Sens Appl Soc Environ. 2024;35:101251. https://doi.org/10.1016/j.rsase.2024.101251.
56. SAS Institute Inc. SAS/STAT® 15.2 user's guide: the GLIMMIX procedure. Cary: SAS Institute Inc.; 2021.
57. SAS Institute Inc. SAS® 9.4 and SAS/STAT® 15.2 software. Cary: SAS Institute Inc.; 2021.
58. SAS Institute Inc. SAS/STAT® 15.3 user's guide: the SURVEYSELECT procedure. Cary: SAS Institute Inc.; 2023.
59. Scarano FR. Ecosystem-based adaptation to climate change: concept, scalability and a role for conservation science. Perspect Ecol Conserv. 2017;15:65–73. https://doi.org/10.1016/j.pecon.2017.05.003.
60. Schowengerdt RA. Remote sensing, models, and methods for image processing. 3rd ed. Burlington: Academic Press; 2007.
61. Sivisaca DCL, Puglla CAY, Passos JRS, Fonseca RCB, Ganga A, Capra GF, et al. Atlantic forest regeneration dynamics following human disturbance cessation in Brazil. Environments. 2024;11:243. https://doi.org/10.3390/environments11110243.
62. Song C, Schroeder T, Cohen W. Predicting temperate conifer forest successional stage distributions with multitemporal Landsat thematic mapper imagery. Remote Sens Environ. 2007;106:228–37. https://doi.org/10.1016/j.rse.2006.08.008.
63. Tamiminia H, Salehi B, Mahdianpari M, Quackenbush L, Adeli S, Brisco B. Google earth engine for geo-big data applications: a meta-analysis and systematic review. ISPRS J Photogramm Remote Sens. 2020;164:152–70. https://doi.org/10.1016/j.isprsjprs.2020.04.001.
64. Tian L, Wu X, Tao Y, Li M, Qian C, Liao L, et al. Review of remote sensing-based methods for forest aboveground biomass estimation: progress, challenges, and prospects. Forests. 2023;14:1086. https://doi.org/10.3390/f14061086.
65. Torabzadeh H, Leiterer R, Hueni A, Schaepman ME, Morsdorf F. Tree species classification in a temperate mixed forest using a combination of imaging spectroscopy and airborne laser scanning. Agric For Meteorol. 2019;279:107744. https://doi.org/10.1016/j.agrformet.2019.107744.
66. Van der Sande MT, Arets EJMM, Peña-Claros M, Hoosbeek MR, Cáceres-Siani Y, Van der Hout P, et al. Soil fertility and species traits, but not diversity, drive productivity and biomass stocks in a Guyanese tropical rainforest. Funct Ecol. 2018;32:461–74. https://doi.org/10.1111/1365-2435.12968.
67. Wani A, Bhat AF, Gatoo AA, Zahoor S, Mehraj B, Najam N, et al. Assessing relationship of forest biophysical factors with NDVI for carbon management in key coniferous strata of temperate Himalayas. Mitig Adapt Strateg Glob Change. 2021;26:1. https://doi.org/10.1007/s11027-021-09937-6.
68. Xie Y, Sha Z, Yu M. Remote sensing imagery in vegetation mapping: a review. J Plant Ecol. 2008;1(1):9–23. https://doi.org/10.1093/jpe/rtm005.
69. Xie Z, Phinn SR, Game ET, Pannell DJ, Hobbs RJ, Briggs PR, et al. Using Landsat observations (1988–2017) and Google Earth engine to detect vegetation cover changes in rangelands - a first step towards identifying degraded lands for conservation. Remote Sens Environ. 2019;232:111317. https://doi.org/10.1016/j.rse.2019.111317.
70. Yin C, Zhao W, Ye J, Muroki M, Pereira P. Ecosystem carbon sequestration service supports the sustainable development goals progress. J Environ Manage. 2023;330:117155. https://doi.org/10.1016/j.jenvman.2022.117155.
71. Yin F, Lewis PE, Gómez-Dans JL. Bayesian atmospheric correction over land: Sentinel-2/MSI and Landsat 8/OLI. Geosci Model Dev. 2022;15:7933–76. https://doi.org/10.5194/gmd-15-7933-2022.
72. Zeng P, Shi J, Huang J, Zhang Y, Zhang W. Component forest above ground biomass estimation using lidar and sardata. IGARSS 2022-2022 IEEE international geoscience and remote sensing symposiyum 2022; https://doi.org/10.1109/IGARSS46834.2022.9883880

Publisher's Note